

Parameter Precision in Global Analysis of Time Resolved Spectra

Ivo H.M van Stokkum

Faculty of Physics and Astronomy,
Vrije Universiteit, De Boelelaan 1081,
1081 HV Amsterdam, The Netherlands
Phone +31 20 4447868 Fax +31 20 4447899 E-Mail: ivo@nat.vu.nl

Abstract - *By means of simulation parameter estimation in global analysis of time resolved spectra was studied. Kinetic, spectral as well as spectrotemporal models were used to describe a system consisting of a mixture of components whose concentrations change with time. The benefits of the spectrotemporal model were found to depend upon the amount of overlap between the time and wavelength properties of the components, and thus where largest when this overlap is small. It was found that an analytical description of a noisy instrument response improves the precision of rate constants estimated by iterative deconvolution.*

I. INTRODUCTION

A system consisting of a mixture of components whose concentrations change with time can be studied by means of time resolved spectroscopy. In the field of molecular photophysics and photochemistry transient absorption and fluorescence spectroscopy following an appropriately short pulse of radiation are widely used. The identification of such a system amounts to the estimation of the parameters which describe the kinetics and spectra of the components. The (impulse) response of the system across wavelength and time results in a so-called time resolved spectrum. According to the Beer-Lambert law the spectroscopic properties of a mixture of components are a superposition of the spectroscopic properties of the components weighted by their concentration. Thus the perfect, noise-free, time resolved spectrum ψ is a superposition of the contributions of the n_{comp} different components:

$$\psi(t, \lambda) = \sum_{l=1}^{n_{\text{comp}}} c_l(t) \varepsilon_l(\lambda) \quad (1)$$

where $c_l(t)$ and $\varepsilon_l(\lambda)$ denote, respectively, the concentration and spectrum of component l . Typically the number of components studied with time resolved spectroscopy is less than ten, whereas the number of different wavelengths or the number of different time instants goes up to thousands. Note that according to (1) a separability of time and wavelength properties is possible. Using a physico-chemical parametric model the data are analysed globally, i.e. with a single model describing the data at all times and wavelengths, in order to improve the parameter precision e.g. [1],[2],[3],[4],[5],[6]. We have used kinetic, spectral as well as spectrotemporal models [2],[6]. The aim of this paper is to study by means of simulation parameter estimation in these three types of models, in particular to investigate the potential benefits of using a more complicated, spectrotemporal model. A special problem which occurs with (global) analysis of single photon timing fluorescence decays is the treatment of the stochastic aspect of the measured instrument response [7] (and references cited therein). Usually it is neglected, but here we show that an analytical description of the instrument response improves the parameter precision.

II. METHODS

The basic model which describes the time evolution of spectra is the following¹:

$$\underline{\psi}_{t_i \lambda_j} = \sum_{l=1}^{n_{\text{comp}}} c_{l t_i} \varepsilon_{l \lambda_j} + \xi_{t_i \lambda_j} \quad (2)$$

$$\underline{\Psi} = C E^T + \Xi \quad (3)$$

¹Notation convention: underlining indicates stochastic variables, uppercase represents matrices, lowercase represents scalars or vectors.

where the $m \times n$ matrix Ψ (with elements Ψ_{t_i, λ_j}) denotes the time resolved spectra, measured at m time instants t_i , and n wavelengths λ_j . c_{ll_i} denotes the concentration of component l at time t_i , $\varepsilon_{l\lambda_j}$ denotes the contribution of component l at wavelength λ_j , and ξ_{t_i, λ_j} denotes a Gaussian distributed stochastic disturbance with zero mean. The c_{ll_i} and $\varepsilon_{l\lambda_j}$ are gathered in the matrices C and E , of dimension $m \times n_{\text{comp}}$ and $n \times n_{\text{comp}}$, respectively. Matrix Ξ is, like Ψ , $m \times n$. We now distinguish three types of model.

A. Kinetic model

The concentrations are described by a kinetic model, which depends upon the nonlinear parameters θ , whereas the spectral parameters of the $n \times n_{\text{comp}}$ matrix E are conditionally linear parameters [8],[9]

$$\underline{\Psi} = C(\theta)E^T + \underline{\Xi} \quad (4)$$

B. Spectral model

The spectra are described by a parametric model, which depends upon the nonlinear parameters θ , whereas the concentration parameters of the $m \times n_{\text{comp}}$ matrix C are conditionally linear parameters

$$\underline{\Psi}^T = E(\theta)C^T + \underline{\Xi}^T \quad (5)$$

Furthermore, the estimated matrices E from (4) and C from (5) can subsequently be fitted with, respectively, a spectral and a kinetic model.

C. Spectrotemporal model

Both the concentrations and the spectra are described by a model, which depends upon the nonlinear parameters θ . Assuming first order kinetics, a matrix of linear parameters A describes the concentrations of the components in terms of a superposition of simple decays which are gathered in the matrix $C(\theta)$.

$$\underline{\Psi} = C(\theta)AE^T(\theta) + \underline{\Xi} \quad (6)$$

With components which decay exponentially the matrix A becomes a diagonal matrix $\text{diag}(a)$.

D. Simulation

We simulated models with two components. The concentrations of the components are described by exponential decays $\exp(-kt)$ with rate parameter k , whereas the spectral shapes are described by a Gaussian in the energy domain

$$\varepsilon(\bar{\nu}) = \bar{\nu}^3 \exp(-\ln 2 [2(\bar{\nu} - \bar{\nu}_{\text{max}})/\Delta\bar{\nu}]^2) \quad (7)$$

with parameters $\bar{\nu}_{\text{max}}$, $\Delta\bar{\nu}$ for, respectively, location and Full Width at Half Maximum (FWHM). Thus the simulated data are a function of eight parameters: for each component four parameters: k , $\bar{\nu}_{\text{max}}$, $\Delta\bar{\nu}$ and amplitude a . To these data normally distributed noise was added.

E. Parameter estimation

The conditionally linear parameters (E in (4), C in (5), A in (6)) can be eliminated in the nonlinear least squares (NLLS) fit by means of the variable projection method [9]. This is especially profitable when their number is large, e.g. in time gated spectra analysed with a kinetic model [2],[5]. The precision of the estimated parameters is summarized by the covariance matrix. The linear approximation covariance matrix of the nonlinear parameters θ is estimated from

$$\text{cov}(\hat{\theta}) = \hat{\sigma}^2 (J^T J)^{-1} \quad (8)$$

where $\hat{\sigma}^2$ denotes the estimated variance and J is the Jacobian of the model function with respect to the parameters θ , evaluated at the NLLS estimate $\hat{\theta}$. We used the Kaufman approximation [9],[10] to calculate this Jacobian. The linear approximation covariance matrix of the conditionally linear parameters contains two contributions. We describe here only the kinetic model case, the case of the spectral model fit is treated analogously. Using standard linear algebra, in particular the matrix inversion lemma, it can be derived that:

$$\text{cov}(\text{vec}(\hat{E}^T)) = \hat{\sigma}^2 I_n \otimes (C^T C)^{-1} + G \text{cov}(\hat{\theta}) G^T \quad (9)$$

where $\text{vec}(\cdot)$ denotes the vector representation, \otimes is the Kronecker product, and $G = (\hat{E} \otimes C^T) \frac{\partial(\text{vec} C)}{\partial \theta}$. Note that the first term on the right hand side of (9) corresponds to the usual linear regression covariance matrix when the nonlinear parameters θ were known, whereas the second term takes into account the uncertainty of $\hat{\theta}$.

F. Profile t plots

To investigate the adequacy of the linear approximation covariance matrix we calculated a likelihood based profile t plot [8]. For a nonlinear model we define the profile t function for parameter θ_p as

$$\tau(\theta_p) = \text{sign}(\theta_p - \hat{\theta}_p) \sqrt{\tilde{S}(\theta_p) - S(\hat{\theta})} / \hat{\sigma} \quad (10)$$

where

$$\tilde{S}(\theta_p) = S(\theta_p, \tilde{\theta}_{-p}) \quad (11)$$

is the profile sum of squares function and $(\theta_p, \tilde{\theta}_{-p}) = (\hat{\theta}_1, \dots, \hat{\theta}_{p-1}, \theta_p, \tilde{\theta}_{p+1}, \dots, \tilde{\theta}_{n_{\text{par}}})$ is the least squares estimate conditional on θ_p . A $1 - \alpha$ likeli-

hood interval for θ_p is now defined as the set of all θ_p for which

$$-t_{df, \alpha/2} \leq \tau(\theta_p) \leq t_{df, \alpha/2} \quad (12)$$

where $t_{df, \alpha/2}$ is the upper $\alpha/2$ quantile for Student's t distribution with df degrees of freedom. Plots of the profile t function versus the studentized parameter as defined in (13)

$$\delta(\theta_p) = \frac{\theta_p - \hat{\theta}_p}{\hat{\sigma} \sqrt{((J^T J)^{-1})_{pp}}} \quad (13)$$

would produce a straight line through the origin with unit slope in the case of a *linear* model. For a *nonlinear* model a plot of $\tau(\theta_p)$ versus $\delta(\theta_p)$ (from (13)) will be curved, the amount of curvature giving information about the nonlinearity of the model.

G. Projection of data

When we assume that the standard deviation of the noise is small, we can reduce the data Ψ by projecting upon the first n_{comp} right or left singular vectors resulting from the Singular Value Decomposition (SVD) of the data matrix:

$$\Psi = \underline{U} \underline{S} \underline{W}^T \quad (14)$$

where \underline{U} and \underline{W} are orthogonal matrices containing the left and right singular vectors, respectively, and \underline{S} is a matrix of zeros except for its diagonal which contains the singular values in non-increasing order. We will describe the procedure for the spectral model fit, the case of the kinetic model fit is treated analogously. Disregarding the stochastic character of the first n_{comp} left singular vectors $\underline{U}_{n_{\text{comp}}}$ the projection gives us

$$\begin{aligned} \underline{\Psi}^T \underline{U}_{n_{\text{comp}}} &= (\underline{W} \underline{S}^T)_{n \times n_{\text{comp}}} = \\ E(\theta) C^T \underline{U}_{n_{\text{comp}}} &+ \underline{\Xi}^T \underline{U}_{n_{\text{comp}}} \end{aligned} \quad (15)$$

Going from (5) to (15) we have reduced our data from $n \times m$ to $n \times n_{\text{comp}}$. Instead of C we must now estimate the $n_{\text{comp}} \times n_{\text{comp}}$ projected concentration parameters $C^T \underline{U}_{n_{\text{comp}}}$. The parameter estimation is completely analogous to the unprojected case. However, to estimate the variance $\hat{\sigma}^2$ from the fit of the projected data the sum of squares of the residuals is augmented with the sum of squares of the remaining singular values, $s_{n_{\text{comp}}+1}, \dots$. The degrees of freedom df are identical to the unprojected case.

III. RESULTS

A. Precision with different types of model

In order to compare the parameter precision we simulated an ensemble of datasets (at least 51) with certain parameters and noise level, and calculated the deviation $\text{dev}(\theta) = \hat{\theta} - \theta$, the difference between the estimated and true value of a parameter, the linear approximation standard error from (8) or (9) and the ratio of these two, which equals minus the studentized parameter (13). From this ensemble of realizations the rms value was calculated and a smoothed probability density was estimated using the Splus function *ksmooth* [11].

The time resolved spectrum was simulated at $m = 51$ time points equidistant in the interval 0-2 ns and $n = 51$ wavelengths equidistant in the interval 350-550 nm. The overlap between the spectra and concentration profiles of the components could be large (EL,CL) or small (ES,CS). The parameters of the three combinations used in the simulations, whose values are inspired by experimental data [5],[6], are summarized in Table I. We

TABLE I

Parameters $k, \bar{v}_{\text{max}}, \Delta \bar{v}$ of components (in $10^9 \text{s}^{-1}, \text{cm}^{-1}$)

Overlap	CSmall (CS)	CLarge (CL)
ESmall (ES)	0.25, 22000, 9000	0.5, 22000, 9000
	1.0, 18000, 8000	0.6, 18000, 8000
ELarge (EL)	0.25, 19000, 9000	
	1.0, 18000, 8000	

studied the parameter precision as a function of the type of model and of the noise level with two combinations of components. With the low noise level the standard deviation of the noise was equal to 6×10^{-3} of the maximum of the data (CS, EL case) or 3×10^{-3} (CL,ES and CS,ES cases). The high noise level was ten times higher. A typical example of a global analysis with the help of a kinetic model of a CL,ES combination data set with low noise is shown in Fig. 1. Note that the fitted curves (dashed lines in Fig. 1a,b) are close to the simulated curves (solid lines). The first two singular values are significantly greater than the remaining ones. Fig. 2 shows the distributions estimated from an ensemble of 751 realizations of this kinetic model fit. The distribution (Fig. 2a) of deviation appears a bit skewed. The studentized parameter distribution deviates from a t_{df} distribution which would apply when the model is linear. The improvement gained with a spectrotemporal model is clearly visible in Fig. 3 (note the differences in scale).

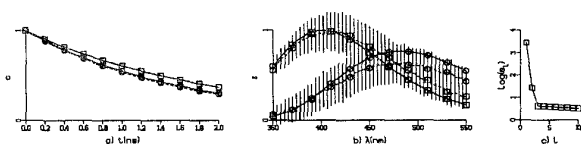


Fig. 1. Global analysis with the help of a kinetic model of CL,ES combination data set with low noise. (a) concentration profiles. Squares and circles indicate first and second component, respectively. Solid and dashed lines indicate true and fitted, respectively. (b) Spectra, vertical bars indicate plus or minus standard error. (c) First ten singular values of data matrix on a logarithmic scale.

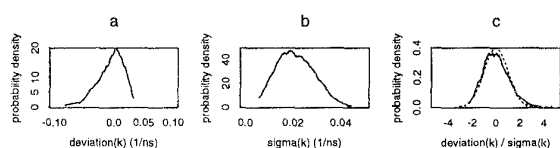


Fig. 2. Distributions estimated from kinetic fit of CL,ES combination with low noise. (a) deviation of estimated rate constant k_1 , (b) standard error, (c) studentized parameter (solid) and t_{df} distribution (dotted).

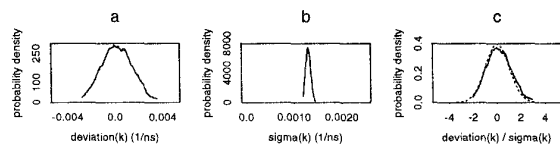


Fig. 3. Distributions estimated from spectrottemporal fit of CL,ES combination with low noise. (a) deviation of estimated rate constant k_1 , (b) standard error, (c) studentized parameter (solid) and t_{df} distribution (dotted).

Note that here the studentized parameter is more closely distributed as t_{df} (Fig. 3c) which indicates that the spectrottemporal model is functionally linear [12]. We thus studied two combinations at two noise levels. The averaged results for the rate constants are collated in Table II. With large spectral overlap (EL) the spectrottemporal model provides only a marginal improvement over the kinetic model. However, with small spectral overlap (ES) the spectrottemporal model is clearly superior, compare the last two columns of Table II. In most cases the rms deviation is approximately equal to the rms standard error (between parentheses). In two exceptional cases, indicated with an asterisk, outliers were present in the standard error estimates.

With the spectral parameters the results for the locations $\bar{\nu}_{\max}$ are collated in Table III. With large temporal over-

TABLE II

Rms deviation (standard error) of rate constants (in 10^6s^{-1})

model	CS, EL		CL, ES	
	$C(\theta)E^T$	$C(\theta)AE^T(\theta)$	$C(\theta)E^T$	$C(\theta)AE^T(\theta)$
low noise	14(14)	13(12)	24(23)	1(1)
	19(20)	18(17)	26(27)	3(3)
high noise	150(130)	130(130)	240(*)	20(17)
	290(190)	200(170)	340(*)	170(110)

TABLE III

Rms deviation (standard error) of $\bar{\nu}_{\max}$ (in 10^1cm^{-1})

model	CS, EL		CL, ES	
	$E(\theta)C^T$	$C(\theta)AE^T(\theta)$	$E(\theta)C^T$	$C(\theta)AE^T(\theta)$
low noise	46(55)	4(4)	12(13)	11(13)
	4(3)	2(2)	3(4)	3(4)
high noise	100(*)	48(44)	160(120)	140(130)
	410(*)	26(25)	36(23)	37(35)

lap (CL) the spectrottemporal model provides only a marginal improvement over the spectral model. Again, with small temporal overlap (CS) the spectrottemporal model is clearly superior, compare columns two and three of Table III. The results for the width parameters $\Delta\bar{\nu}$ are comparable. With low noise the kinetic or spectral fits using projected data produced results identical to the fits with unprojected data. With high noise the results were only slightly worse. To study robustness against systematic deviations from the model assumptions we simulated data subject to time jitter, a common problem with time gated spectra [5],[6]. We simulated a uniformly distributed time jitter (-0.05,0.05) ns. Besides the kinetic and spectrottemporal model we also used a spectral model of which the estimated concentration profiles were subsequently fitted with a kinetic model. It is clear from Table IV that with low noise the last approach produces the most precise estimates of the parameters, thus confirming [6]. However, with high noise the time jitter becomes relatively less important, and the spectrottemporal model is again superior.

B. Precision with instrument response noise

Next, we investigate by means of a simulation study the effect of noise in the instrument response upon the precision of rate constants estimated by iterative reconvolu-

TABLE IV
Rms deviation (standard error) of rate constants (in 10^6s^{-1}); time jitter present

		CS, ES		
model		$C(\theta)E^T$	$C(\theta)AE^T(\theta)$	$E(\theta)C^T ; C(\theta)$
low noise		10(7)	4(3)	3(2)
		65(16)	54(11)	20(10)
high noise		43(45)	20(22)	42(11)
		110(97)	76(70)	623(252)

tion, a well known problem in the (global) analysis of single photon timing fluorescence decays.

We simulated the measurement of the Gaussian shaped instrument response of 141 ps FWHM with Poisson statistics, its peak value being 5000. An exponential decay with $k = 2 \times 10^{10} \text{ s}^{-1}$ convolved with the true instrument response was simulated at $m = 161$ time points equidistant in the interval 0-800 ps with Poisson statistics, its peak value being either 22000 or 2200. In a much more difficult estimation situation a second component with a decay rate constant of $k = 1 \times 10^{10} \text{ s}^{-1}$ and equal amplitude was added. The rms deviations of the rate constant estimates when fitting with an analytical expression for the instrument response or when the observed, stochastic instrument response was used in combination with numeric convolution [13] are collated in Table V. With little noise (first, third and fourth row) the analytical approach provides a clear improvement (up to 40%) over the numeric convolution with the observed, stochastic instrument response. With more noise (second, fifth and sixth row) the improvement becomes relatively smaller, on the order of 10%. Note further that in general the rms standard errors are somewhat smaller than the rms deviations, and thus are too optimistic. Increase of the peak value by a factor of ten corresponds roughly to an improvement in precision by a factor of 2-4, which includes $\sqrt{10}$.

The applicability of the use of an analytically described instrument response in iterative reconvolution depends upon the availability of a suitable analytical description. A versatile candidate function is (a linear combination of) $\alpha[(t-\mu)/(\gamma\tau)]^\gamma \exp(\gamma - (t-\mu)/\tau)$ with parameters $\alpha, \gamma, \mu, \tau$ for amplitude, shape, location, width. Convolution of this function with an exponential decay results in the confluent hypergeometric function.

C. Profile τ plots

Profile τ plots for the rate parameters estimated with the CL,ES combination already analysed in Fig. 1 are shown

TABLE V
Rms deviation (standard error) of rate constants (in 10^9s^{-1})

rate	peak	analytical instrument response	noisy instrument response
20	22000	0.054(45)	0.079(50)
20	2200	0.153(138)	0.165(146)
20	56000	1.43(1.33)	2.41(1.63)
10		0.26(0.24)	0.30(0.26)
20	5600	5.0(4.5)	5.4(5.0)
10		1.23(1.10)	1.33(1.10)

as solid lines in Fig. 4. Note that in this case of close decay rate constants the curves deviate from the dashed straight line which indicates nonlinearity of the model and thus inadequacy of the linear approximation standard errors. E.g. the 99% likelihood interval for $k_1 \equiv \theta_1$ is asymmetric around the least squares estimate and equal to (0.429, 0.524) whereas the linear approximation interval is 0.495 ± 0.051 .

For comparison we show the profile τ plots for the rate parameters estimated with the CS,ES combination and the same, low, noise level in Fig. 5. Note that in this small overlap case the solid and dashed line are hardly distinguishable, indicating that in this case the model is functionally linear [12]. With a CS,EL combination the profile τ plots deviate a little bit more from the dashed line than in Fig. 5 (not shown) indicating a slight nonlinearity.

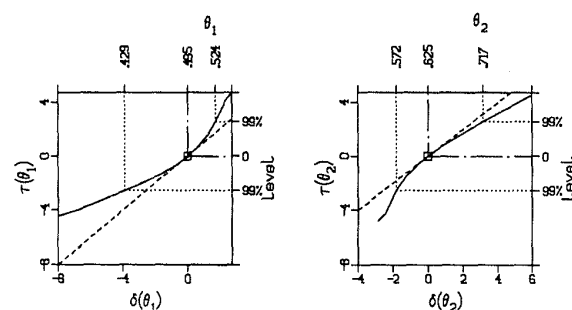


Fig. 4. Plots of profile τ function $\tau(\theta)$ versus studentized parameter $\delta(\theta)$ (solid lines) for the rate parameters estimated in Fig. 1. Dotted horizontal and vertical lines indicate derivation of 99% likelihood interval around least squares estimate (squares). Dashed line represents $\tau(\theta) = \delta(\theta)$ which is appropriate for linear models.

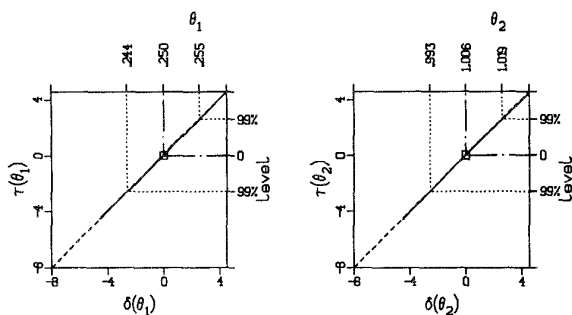


Fig. 5. Plots of profile t function $\tau(\theta)$ versus studentized parameter $\delta(\theta)$ (solid lines) for the rate parameters estimated from a CS,ES combination. Dotted horizontal and vertical lines indicate derivation of 99% likelihood interval around least squares estimate (squares). Dashed line represents $\tau(\theta) = \delta(\theta)$ which is appropriate for linear models.

IV. CONCLUSIONS

The improvement in parameter precision that can be achieved by a spectrotemporal model depends upon the overlap between component properties. Compared to a kinetic model the improvement is largest when the spectral overlap is small (Table II). Compared to a spectral model the improvement is largest when the temporal overlap is small (Table III).

When systematic errors are present the choice of models should take these into account. E.g. with time jitter (a common problem with time gated spectra) a spectral model is least sensitive to the amplitude fluctuations. With low noise subsequent kinetic analysis of the thus estimated concentration profiles provides the best results. However, with high noise the time jitter becomes relatively less important and the spectrotemporal model is superior again (Table IV).

With ideal noise data reduction by projection upon the first n_{comp} singular vectors does not harm the parameter precision. However, with structured noise, e.g. near an isosbestic point in difference absorption spectroscopy (Van Brederode and Van Stokkum, unpublished observations), the noise can dominate the n_{comp} -th singular vectors thus causing failure of the fits with projected data.

The analytical description of the instrument response improves the precision of rate constants estimated by iterative reconvolution. The improvement depends again upon the noise level of the data. The improvement is largest with low noise in the data where the stochastic errors in the observed instrument response are relatively more important (Table V).

Profile t plots can be calculated to investigate the degree

of model nonlinearity. When the data can be reduced by projection upon the first n_{comp} singular vectors this time consuming calculation can be speeded up considerably. The adequacy of the linear approximation covariance matrix depends again upon the overlap between component properties, in accordance with [14]. With small overlap in both the spectral and temporal domain the model behaves functionally linear (Fig. 3, Fig. 5) whereas with large temporal overlap the profile t plots for the kinetic parameters clearly show nonlinearity (Fig. 2, Fig. 4).

ACKNOWLEDGMENT

Dr H.J.W. Spoelder is thanked for critical reading of the text.

REFERENCES

- [1] J.M. Beechem, E. Gratton, M. Ameloot, J.R. Knutson and L. Brand, "The global analysis of fluorescence decay data: second generation theory and programs," in *Fluorescence Spectroscopy: Principles*, vol. 2, J.R. Lakowicz, Ed. New York: Plenum Press, 1992, pp. 241-305.
- [2] W.D. Hoff, I.H.M. van Stokkum, H.J. van Ramesdonk, M.E. van Brederode, A.M. Brouwer, J.C. Fitch, T.E. Meyer, R. van Grondelle and K.J. Hellingwerf, "Measurement and global analysis of the absorbance changes in the photocycle of the photoactive yellow protein from *Ectothiorhodospira halophila*," *Biophys. J.*, vol. 67, pp. 1691-1705, 1994.
- [3] J.R. Knutson, J.M. Beechem and L. Brand, "Simultaneous analysis of multiple fluorescence decay curves: A global approach," *Chem. Phys. Lett.*, vol. 102, pp. 501-507, 1983.
- [4] K.-H. Müller and Th. Plesser, "Variance reduction by simultaneous multi-exponential analysis of data sets from different experiments," *Eur. Biophys. J.*, vol. 19, pp. 231-240, 1991.
- [5] I.H.M. van Stokkum, A.M. Brouwer, H.J. van Ramesdonk and T. Scherer, "Multiresponse parameter estimation and compartmental analysis of time resolved fluorescence spectra," *Proc. Kon. Ned. Akad. v. Wetensch.*, vol. 96, pp. 43-68, 1993.
- [6] I.H.M. van Stokkum, T. Scherer, A.M. Brouwer and J.W. Verhoeven, "Conformational dynamics of flexibly and semirigidly bridged electron donor-acceptor systems as revealed by spectrotemporal parameterization of fluorescence," *J. Phys. Chem.*, vol. 98, pp. 852-866, 1994.
- [7] Z. Bajzer, A. Zelić and F.G. Prendergast, "Analytical approach to the recovery of short fluorescence lifetimes from fluorescence decay curves," *Biophys. J.*, vol. 69, pp. 1148-1161, 1995.
- [8] D.M. Bates and D.G. Watts, *Nonlinear Regression Analysis and Its Applications*. New York: Wiley, 1988.
- [9] G.H. Golub and R.J. LeVeque, "Extensions and uses of the variable projection algorithm for solving nonlinear least squares," in *Proceedings of the 1979 Army Numerical Analysis and Comp. Conf.*, ARO Report 79-3, 1979, pp. 1-12.
- [10] L. Kaufman, "A variable projection method for solving separable nonlinear least squares problems," *BIT*, vol. 15, pp. 49-57, 1975.
- [11] *Splus Reference Manual*, Statistical Sciences Inc., Seattle, 1991.
- [12] J. Brooks, D.G. Watts, K.K. Soneson and P. Hensley, "Determining confidence intervals for parameters derived from analysis of equilibrium analytical ultracentrifugation data," *Meth. Enzymol.*, vol. 240, 459-478.
- [13] J.M. Bouchy, J.Y. Jezequel, J.C. Andre and J. Bordet, "Problems arising from the quantization of the data in the mathematical treatment of single photon counting experiments," in *Deconvolution and reconvolution of analytical signals. Application to fluorescence spectroscopy*, 1982, pp.393-409.
- [14] R. Pribić, I.H.M. van Stokkum and A. van den Bos, "Inference regions of nonlinear parameters in global analysis," in *Proceedings SYSID '94, 10th IFAC Symposium on System Identification*, M. Blanke and T. Söderström, Eds. Copenhagen: Danish Automation Society, 1994, pp. 2.423-2.428.